

MICROCOPY RESOLUTION TEST CHART
NATIONAL BUREAU OF STANDARDS-1963-A

2

AD-A167 810

NAVAL POSTGRADUATE SCHOOL

Monterey, California



DTIC
ELECTE
MAY 22 1986
S E D

THESIS

DTIC FILE COPY

A DIAGNOSTIC INVESTIGATION OF
EXPLOSIVE MARITIME CYCLOGENESIS
DURING FGGE

by

Darrell H. Smith

March 1986

Thesis Advisor: C. H. Wash

Approved for public release; distribution is unlimited.

86 5 21 079

REPORT DOCUMENTATION PAGE

1a. REPORT SECURITY CLASSIFICATION			1b. RESTRICTIVE MARKINGS			
2a. SECURITY CLASSIFICATION AUTHORITY			3. DISTRIBUTION/AVAILABILITY OF REPORT Approved for public release: distribution is unlimited			
2b. DECLASSIFICATION/DOWNGRADING SCHEDULE						
4. PERFORMING ORGANIZATION REPORT NUMBER(S)			5. MONITORING ORGANIZATION REPORT NUMBER(S)			
6a. NAME OF PERFORMING ORGANIZATION Naval Postgraduate School		6b. OFFICE SYMBOL (if applicable) Code 63	7a. NAME OF MONITORING ORGANIZATION Naval Postgraduate School			
6c. ADDRESS (City, State, and ZIP Code) Monterey, California 93943-5100			7b. ADDRESS (City, State, and ZIP Code) Monterey, California 93943-5100			
8a. NAME OF FUNDING/SPONSORING ORGANIZATION		8b. OFFICE SYMBOL (if applicable)	9. PROCUREMENT INSTRUMENT IDENTIFICATION NUMBER			
8c. ADDRESS (City, State, and ZIP Code)			10. SOURCE OF FUNDING NUMBERS			
			PROGRAM ELEMENT NO.	PROJECT NO.	TASK NO.	WORK UNIT ACCESSION NO.
11. TITLE (Include Security Classification) A Diagnostic Investigation of Explosive Maritime Cyclogenesis During FGGE						
12. PERSONAL AUTHOR(S) Smith, Darrell H.						
13a. TYPE OF REPORT Master's Thesis		13b. TIME COVERED FROM TO		14. DATE OF REPORT (Year, Month, Day) 1986 March		15. PAGE COUNT 55
16. SUPPLEMENTARY NOTATION (EXPLICIT CLASSIFICATION MEDIUM RANGE FORECASTS)						
17. COSATI CODES			18. SUBJECT TERMS (Continue on reverse if necessary and identify by block number)			
FIELD	GROUP	SUB-GROUP	Explosive cyclogenesis; vorticity advection; mass divergence; static stability; potential temperature; absolute vorticity; THESE S. ←			
19. ABSTRACT (Continue on reverse if necessary and identify by block number) A collection of explosive and non-explosive storm groups are selected from the western North Atlantic Ocean and western North Pacific Ocean, during the period 17 January 1979 to 23 February 1979. Explosive cyclogenesis is defined as having a mean sea level pressure fall of 1 mb h for 24 h. Using ECMWF analyses with FGGE SOP-1 data, the storm environment properties of both storm types are analyzed and compared. Storm environment properties include static stability, layer averaged potential temperature, low level vorticity, vorticity advection, mean and eddy modes of vorticity transport, divergence and kinematic vertical velocities. These properties are compared between the cyclone types at 0 h, 12 h and 24 h periods as well as the overall 24 h average. The largest differences between the explosive group and the non-explosive group are found in the upper level divergence and vorticity advection. The explosive systems are warmer; however, static stabilities of the two groups are quite similar. Keywords:						
20. DISTRIBUTION/AVAILABILITY OF ABSTRACT <input type="checkbox"/> UNCLASSIFIED/UNLIMITED <input type="checkbox"/> SAME AS RPT. <input type="checkbox"/> DTIC USERS			21. ABSTRACT SECURITY CLASSIFICATION Unclassified			
22a. NAME OF RESPONSIBLE INDIVIDUAL Carlyle P. Wash			22b. TELEPHONE (Include Area Code) 409-616-2206		22c. OFFICE SYMBOL 6274	

Approved for public release; distribution is unlimited.

A Diagnostic Investigation of
Explosive Maritime Cyclogenesis
During FGGE

by

Darrell H. Smith
Lieutenant Commander, United States Navy
B.S., University of Oklahoma, 1976

Submitted in partial fulfillment of the
requirements for the degree of

MASTER OF SCIENCE IN METEOROLOGY AND OCEANOGRAPHY

from the

NAVAL POSTGRADUATE SCHOOL
March 1986

Author:

Darrell H. Smith

Darrell H. Smith

Approved by:

C. H. Wash

C. H. Wash, Thesis Advisor

R. L. Elsberry

R. L. Elsberry, Second Reader

R. J. Renard

R. J. Renard, Chairman,
Department of Meteorology

John N. Dyer

John N. Dyer,
Dean of Science and Engineering

ABSTRACT

A collection of explosive and non-explosive storm groups are selected from the western North Atlantic Ocean and western North Pacific Ocean during the period 17 January 1979 to 23 February 1979. Explosive cyclogenesis is defined as having a mean sea-level pressure fall of 1 mb h^{-1} for 24 h. Using ECMWF analyses with FGGE SOP-1 data, the storm-environment properties of both storm types are analyzed and compared. Storm environment properties include static stability, layer-averaged potential temperature, low-level vorticity, vorticity advection, mean and eddy modes of vorticity transport, divergence and kinematic vertical velocities. These properties are compared between the cyclone types at 0 h, 12 h and 24 h periods as well as the overall 24 h average. The largest differences between the explosive group and the non-explosive group are found in the upper-level divergence and vorticity advection. The explosive systems are warmer; however, static stabilities of the two groups are quite similar.

Accession For	
NTIS GRA&I	<input checked="" type="checkbox"/>
DTIC TAB	<input type="checkbox"/>
Unannounced	<input type="checkbox"/>
Justification	
By _____	
Distribution/	
Availability Codes	
Dist	Avail and/or Special
A-1	



TABLE OF CONTENTS

I. INTRODUCTION 5

II. REVIEW OF RECENT STUDIES 9

III. DATA DESCRIPTION 14

IV. CYCLONE SELECTION 16

V. STORM-ENVIRONMENT DIAGNOSTIC CALCULATIONS 22

VI. RESULTS 27

 A. INTRODUCTION 27

 B. 24 H AVERAGE STORM COMPARISON 28

 C. TIME TENDENCY OF LOW-LEVEL CIRCULATION 30

 D. TIME TENDENCY OF UPPER-LEVEL FORCING 31

 E. TIME TENDENCY OF THE THERMAL STRUCTURE 34

 F. SUMMARY 35

VII. CONCLUSIONS AND RECOMMENDATIONS 48

LIST OF REFERENCES 50

INITIAL DISTRIBUTION LIST 53

I. INTRODUCTION

Extraordinarily rapid deepening of maritime low pressure systems and associated poor numerical weather predictions have been recently documented (Sanders and Gyakum, 1980; Anthes et al., 1983; and others). These explosive cyclogenesis events are characterized by a deepening rate adjusted for latitude of at least 1 mb h^{-1} over a 12 or 24 hour period. Storms that develop so rapidly and attain near hurricane-force winds are a serious threat to all maritime activities. The inability of current operational numerical models to predict accurately the rapid deepening can be attributed to the obvious lack of data over the ocean, the difficulty of parameterizing smaller scale physical processes, as well as accurately analyzing large-scale processes important to rapid development.

The physical processes responsible for the rapid deepening of low pressure systems are the subject of controversy. In their climatological study, Sanders and Gyakum (1980) found that maritime explosive cyclogenesis occurred primarily north of the jet stream and nearly 400 nautical miles downstream of mobile upper-level troughs. This implies that some type of upper-level forcing is important for explosive cyclogenesis. For the Presidents' Day Storm of 18-19 February 1979, Uccellini et al. (1984) utilized isentropic analyses of the upper troposphere to illustrate the role of the subtropical jet streak (STJ) as a possible upper-level forcing mechanism in conjunction with an ageostrophic, low-level jet (LLJ). Further examination of the Presidents' Day storm by Uccellini et al. (1985) confirmed the influence of an upstream trough associated with the polar jet (PJ) on this rapid cyclogenesis case. In other studies of the Presidents' Day storm, Bosart (1981) and

Bosart and Lin (1985) associated the rapid deepening of the cyclone with the destabilization of the boundary layer by sensible and latent heat fluxes seaward of the eastern coast of the United States. Cold air dammed against the eastern slopes of the Appalachians was also present. The cyclone developed on the pre-existing coastal front and moved toward the north-northeast into a region of greater upper-level support which caused further deepening. Diagnostic investigations of separate oceanic explosive cyclogenesis events by Cook (1983) and Calland (1983), using data from the First GARP Global Experiment (FGGE), illustrated the significant interaction between the boundary layer and upper-level jet features .

Gyakum (1983b) attributed the explosive development of the 10-11 September 1978 storm (QE II Storm) to the release of latent heat. Chen et al. (1985) also found that latent heat enhanced cyclogenesis in the 13-15 February 1975 storm in the western North Pacific Ocean. Latent heat is also an important process in the development of tropical cyclones (Ooyama, 1969; and others). The fact that many explosive oceanic lows have exhibited features such as an eye and strong winds similar to tropical cyclones led many to believe that latent heat release may be an important mechanism for explosive cyclogenesis.

The thrust of this research is to study further the mechanisms of explosive oceanic cyclogenesis. The thesis objective is to investigate the importance of the upper-level forcing mechanisms and the boundary layer characteristics during the initial rapid deepening periods of maritime explosive cyclogenesis events. In this study, diagnostic calculations for a group of explosive lows will be compared with those from a group of non-explosively deepening systems. Cyclones are selected from the western North Pacific Ocean and the western North Atlantic Ocean. These

regions coincide with the areas of maximum frequency of explosive cyclogenesis (Sanders and Gyakum, 1980). The developmental characteristics of each low pressure system which passes through either area will be evaluated. Upper-level forcing measures to be evaluated include positive vorticity advection and mass divergence. The degree of reduced stability ($d\theta/dp$), thermal structure and absolute vorticity of the lower portion of the troposphere will also be evaluated in association with upper-level forcing.

Although criteria exists for a rapidly deepening extra-tropical cyclone, the limits for non-explosive cyclogenesis events must also be clearly stated. Lows that failed to meet the explosive deepening standards will be designated as non-explosive events. The analysis period for both types of storms will cover the initial 24-hour period in which the central pressure of the low was observed to fall in accordance with the established criteria.

It is difficult to obtain good three-dimensional data sets of oceanic storm systems. Most systems studied to date either were coastal (with land radiosondes) or involved considerable data assumptions (e.g. Gyakum, 1983a). Analyses from the European Centre for Medium-range Weather Forecasts (ECMWF), based on data gathered during FGGE, are used to obtain the most complete data set as possible for this study.

Chapter II will summarize the current research efforts on explosive maritime cyclogenesis. Emphasis will be placed upon the different causes of these maritime oceanic atmospheric events. A description of data acquisition will be contained in Chapter III. The process of selection of the explosive and non-explosive cyclones will be discussed in Chapter IV. Processing of the data utilizing the Quasi-Lagrangian Diagnostic scheme is described in Chapter V. Chapter VI presents the results of the comparison of the

two storm types and their associated properties during the initial development stage. Chapter VII discusses the conclusions of this study of the comparative cyclone diagnostics.

II. REVIEW OF RECENT STUDIES

The physical processes that cause maritime explosive cyclogenesis are not well understood. To gain knowledge of these processes, observations must be achieved on horizontal and vertical scales sufficient to evaluate the rapid deepening processes and forcing. The fact that these events take place over the open ocean makes the collection of sufficient data difficult. The ability to accurately forecast these explosive low pressure systems will follow the understanding of the processes which trigger them. To this end, the numerous case studies that have investigated these rapid deepening low pressure systems have resulted in a number of potential causes for these events.

Sanders and Gyakum (1980) compiled the first extensive data base of explosive maritime cyclogenesis during the period from September 1976 through May 1979. Their climatological study emphasizes the role of the synoptic weather pattern combined with the ocean influence to aid in explaining where the genesis takes place, and to a certain extent, the factors which aid in the development. One of the primary results is that these maritime events occur near or over large gradients of sea-surface temperatures associated with western boundary ocean currents (Figure 2.1). Very few of the explosive deepening events occur in regions without significant sea-surface temperature gradients. As cold continental air moves over the warmer ocean surface, intense latent and sensible heat exchange occurs, which results in the destabilization of the lower atmosphere. These vertical fluxes are well documented in case studies such as Bosart (1981) and clearly indicate a decrease in the baroclinity with subsequent lowering of static stability. In several numerical simulations of cyclogenesis (Anthes et

al., 1983; Chang et al., 1984), a warm core structure evolved when latent heat was added. Anthes et al. (1983) demonstrated that a deeper surface cyclone was also produced when latent heat was included. Chen et al. (1985) found that the cyclone of 13-15 February 1975 also had a warm core.

More conclusively, Sanders and Gyakum (1980) found that rapid deepening low pressure systems occur approximately 400 n mi downstream from a mid-level trough to the west and south of the surface cyclone, which creates an area of divergence near or over the surface low. Bosart (1981) and Uccellini et al. (1985) found that the primary cause for the rapid deepening of the Presidents' Day storm of 18-19 February 1979 was due to a mid-tropospheric short wave in conjunction with low tropospheric warm advection. Chen et al. (1985) noted in their case study of an explosive cyclone off the coast of Japan that it was not until the surface perturbation linked up with the upper-level trough that explosive deepening occurred. Rapid pressure falls at or near the surface due to the increase of upward vertical motion is reflected by the increase of low-level convergence.

Other studies have emphasized the presence of a jet streak as a signature of the upper-level support. Bosart and Lin (1984) in their diagnostic analysis of the Presidents' Day storm compared vertical velocities calculated by various methods. They also found that the primary upper-level forcing was provided by the jet streak. In another study of the Presidents' Day storm, Uccellini et al. (1985) demonstrated the significance of the mid-level jet streak and its effect on the rapid deepening of the storm.

In an investigation of an explosive cyclogenesis event over the North Pacific Ocean during 12-17 January 1979 using FGGE analyses, Calland (1983) also concluded that an

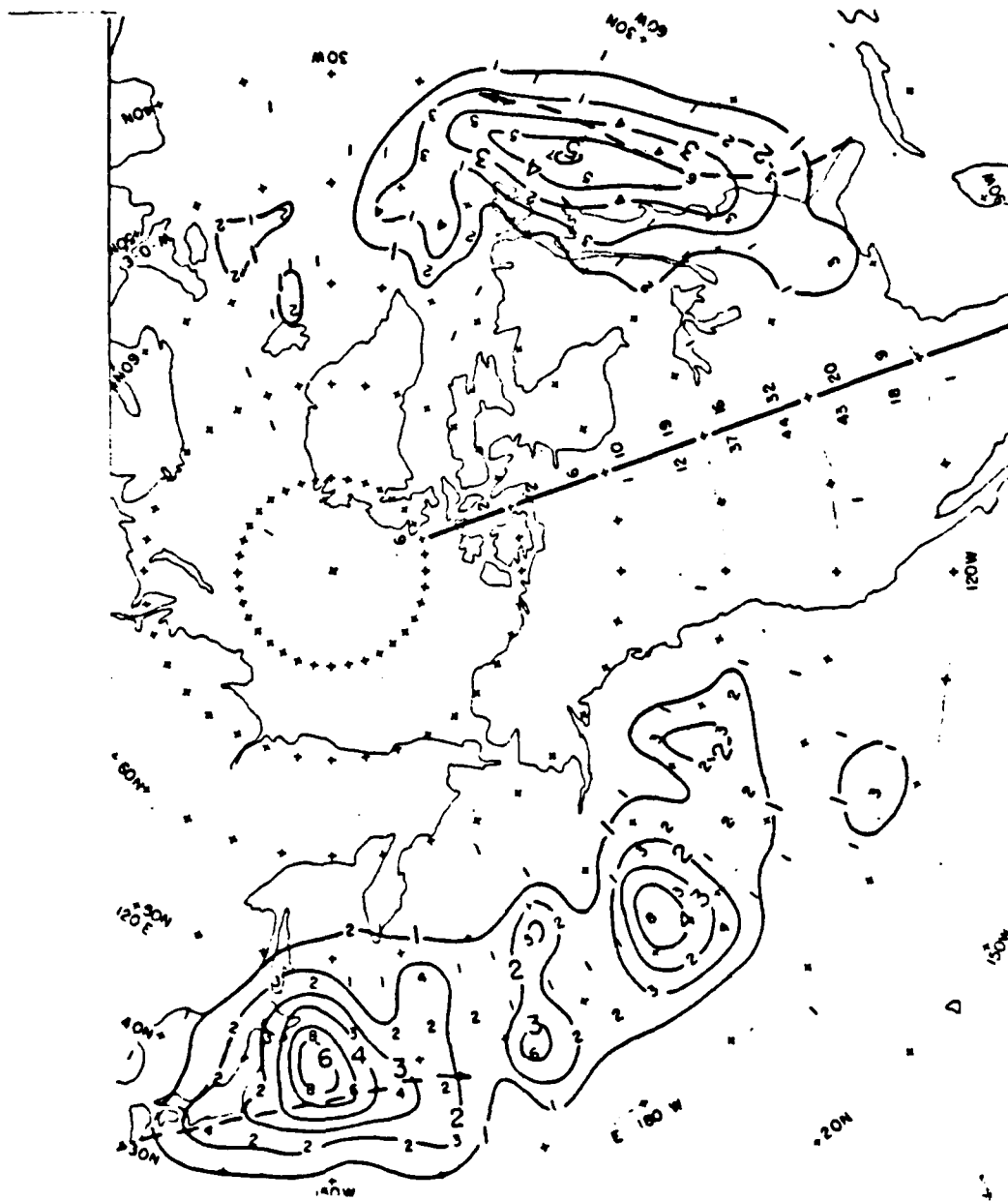


Fig. 2.1 Distribution of explosive cyclogenesis events during three cold seasons. Raw non-zero frequencies appear in each $5^\circ \times 5^\circ$ quadrilateral of latitude and longitude. Isopleths represent smoothed frequencies, obtained as one-eighth of the sum of four times the raw central frequency plus the sum of the surrounding raw frequencies. The column of numbers to the left and right of the heavy line along longitude 90° W represent, respectively, the normalized frequencies for each 5° latitude belt in the Pacific Ocean and Atlantic Ocean regions, using a normalization of $(\cos 42.5^\circ / \cos \phi)$. Heavy dashed lines represent the mean winter position of the Kuroshio and the Gulf Stream (after Sanders and Gyakum, 1980).

upper-level jet streak with associated mass divergence was responsible for the rapid deepening of the surface low. In a similar FGGE study of another explosive maritime event on 26 January 1979, Cook (1983) attributed the spin-up of the cyclone to the presence of an upper-level jet maximum and of reduced low-level stability.

In a study of weak versus strong synoptic-scale forcing, Pagnotti and Bosart (1984) suggest that in addition to latent heating and warm advection, differential cyclonic vorticity advection is needed for rapid deepening to occur. Additionally, both weak and strong synoptic-scale forcing events displayed a maximum of vertical motion at 800 mb. In a response to this study, Uccellini (1984) pointed out that in the absence of a short-wave trough with positive vorticity advection in the mid-troposphere (such as the weak forcing case), the advection shear vorticity associated with the jet streak plays the same role as the positive vorticity advection in the strong case.

Recently Rogers and Bosart (1985) have used composited ocean weather-ship data from 1965 to 1974 to determine the three-dimensional structure of explosive North Atlantic Ocean cyclones. Their composite analyses indicate the rapidly developing cyclone is initially confined to the lower troposphere. However, they point out the strength of upper-level features may have been smoothed out in the data averaging. Evidence of a deep layer of baroclinity and of low static stability are also found in agreement with the above studies. While this study focuses on the differences between explosive and non-explosive cyclones for the North Atlantic Ocean and Pacific Ocean, Rogers and Bosart (1985) focuses only on explosive cyclogenesis in the North Atlantic Ocean. An important difference is that Rogers and Bosart (1985) construct average fields by compositing individual observations from many different storms whereas this study

composites horizontal analyses from a limited set of explosive cyclones and is contrasted with a limited set of non-explosive cyclones.

It is clear from the above literature discussion that the physical processes which determine whether a surface perturbation deepens rapidly or not have not been precisely defined. Important physical processes identified by these studies are the basis for this thesis hypothesis. That is, explosive development of surface low pressure systems at sea occurs when there exists significant upper-level forcing juxtaposed over an area of low stability in conjunction with a weak low-level disturbance. Then, and only then, will rapid deepening of the surface low pressure system occur. This thesis will evaluate the relative magnitudes of these processes by utilizing budget analyses of a number of explosive and non-explosive cyclones.

III. DATA DESCRIPTION

Open-ocean areas where these intense weather systems develop frequently are data sparse. Because of these, a world-wide effort, FGGE, was undertaken during 1978-1979 to compile the most extensive observational record of the atmosphere. Data archived from FGGE were used for this research.

During FGGE, observations included surface (sea, land and drifting buoys) reports and rawinsondes, in addition to dropsondes, aircraft, pilot balloons and satellite measurements. More than 7000 temperature sounding profiles per day from two polar orbiting satellites and 6000 cloud drift winds from five geostationary satellites were included in the analyses. This fulfilled the prerequisite for a complete set of global measurements of the atmosphere to be taken twice daily with at least a 500 km resolution horizontally. This intensive worldwide effort resulted in the most complete set of meteorological parameters ever collected on such a large scale (Halem et al., 1982).

The data management and processing were divided into three different levels of control. Level I consisted of the raw observations acquired from the various instrument platforms. Level II-b ("b" denotes data collected within a cut-off period of three months) was the result of taking Level I data and transforming it into basic meteorological parameters, which comprises the fundamental product of FGGE. The final analysis and transformation into meteorological fields (Level III-b) was accomplished by the European Centre for Medium-range Forecasts (ECMWF), Geophysical Fluid Dynamics Laboratory (GFDL) and NASA/Goddard Laboratory for Atmospheres.

At the ECMWF, assimilation was accomplished using a multivariate optimum interpolation analysis with a normal mode initialization algorithm. The high resolution forecast fields provided the necessary input as the first-guess field for subsequent analyses and prognoses. Optimum interpolation involves the estimation of the necessary weighting factors assigned to each observation used in the analysis. The weighting factors are dependent upon the error characteristics of the observations, the first-guess field and the density distribution of the observational network. The main assumption used by the assimilation system was that geostrophic balance existed between the geopotential height gradients and the wind components and thus assured that the first-guess field will be nearly geostrophic at high latitudes and locally non-divergent (Bengtsson et al., 1982).

During Special Observing Periods, ECMWF Level III-b analyses were archived every six hours for all mandatory levels plus additional levels in the stratosphere. The horizontal resolution of the analyses is 1.875 degrees latitude and longitude. The final data set consists of the basic meteorological fields: sea-level pressure, geopotential heights and horizontal wind components. In addition to this set are the derived parameters: temperature, vertical motion and relative humidity (Bengtsson et al., 1982). Temperatures were calculated from the initialized geopotential analyses, via the hydrostatic relation and interpolated back to the standard pressure levels (Bjorheim et al., 1981). Relative humidities were obtained from precipitable water analyses (Bengtsson et al., 1982).

These data sets will be used in the calculation of storm-environment parameters. The following chapter discusses the storm selection process and presents the final list of cyclones to be analyzed.

IV. CYCLONE SELECTION

Climatological records indicate that the maximum frequency of maritime cyclogenesis occurs in the western regions of the North Pacific and North Atlantic Oceans (Petterssen, 1956). The frequencies of intense events, both spatially and temporally, were documented by Sanders and Gyakum (1980) and updated more recently by Roebber (1984). Both research studies indicated the maximum occurrence of cyclogenesis was during the winter months. Because of these findings, the efforts of this study focus on the western portions of the North Pacific and North Atlantic Oceans during winter 1979. Specifically, the boundaries for the Pacific area extend from 20° N to 60° N. The western side of the area is bounded by 120° E and the eastern boundary is 180° (Figure 4.1). The area selected for the Atlantic Ocean is bounded by 30° N and 60° N. Eastern and western boundaries are 40° W and 85° W, respectively.

This study will investigate all explosive and non-explosive storms from 1800 GMT 17 January 1979 through 0600 GMT 28 February 1979. This period was chosen specifically to use analyses during the first Special Observing Period of FGGE. The amount of observational data gathered during this period is significantly higher than the observational data normally collected at synoptic times. This increase in data coverage, plus the use of a complex data assimilation scheme, has produced high-quality, three-dimensional analyses over the oceans (Halem et al., 1982).

Initial selection of storms was taken from the final sea-level pressure analyses produced by the National Meteorological Center (NMC). To be selected, a storm must have had one closed isobar throughout the initial 24 h development period. To distinguish between explosive and

non-explosive cyclogenesis, pressure falls were extracted and tabulated. Falls in central pressure of 24 mb or greater in 24 h (adjusted for latitude) were categorized as explosive events. Storms that deepened, but failed to meet the explosive deepening criterion, were categorized as non-explosive events. The adjustment factor ($\sin \phi / \sin 60^\circ$) for latitudinal variations in deepening rates assumed a standard latitude of 60° , as used by Sanders and Gyakum (1980). Roebber (1984) used an average latitude of 42.5° vice 60° for normalizing the deepening rates of low pressure systems. Only those storms that deepened over the ocean were considered. If a storm regenerated after an initial explosive deepening period, only the first period of rapid deepening was considered. Secondary generation was not included because other physical processes attributed to this stage might differ significantly from the processes responsible for the initial rapid deepening.

This initial list of explosive and non-explosive extratropical cyclones was comprised of low pressure systems taken directly from the NMC final analyses. As a reference to ensure a complete selection of explosive cyclones, the record of explosive lows by Sanders and Gyakum (1980) was also consulted. All explosive cyclones identified by these authors coincided with those initially selected. Using the initial list of storms from the NMC analyses, the ECMWF Level III-b analyses were used to verify the pressure falls and the storm positions from the NMC analyses. Since all budget calculations will use the three-dimensional ECMWF gridded data, the final list of all extratropical storms was compiled using the ECMWF Level III-b gridded data as the definitive analysis.

The complete list of explosive and non-explosive cyclogenesis is found in Table 1. The geographical positions of each low pressure system for the North Pacific area and the

North Atlantic area are plotted in Figure 4.1 and Figure 4.2, respectively.

Referring to Table 1 in Chapter IV, NP10, NP11 and NA3 were initially considered explosive deepeners using the NMC final surface analyses (note associated 24 h pressure changes according to NMC and ECMWF). Sea-level pressure falls from ECMWF analyses of the these three storms failed to meet the criteria for explosive deepening. Consequently, all three storms were categorized as non-explosive storms for the final list. P7 was the only storm from either ocean area that was originally classified as a non-explosive low and was subsequently shifted to the explosive category.

Some comments are worth noting concerning the final list of storms used for this study and their positions. First, it is not surprising to find that the majority of storms are found near western boundary currents. The Kuroshio and Gulf Stream currents are major areas of sensible and latent heat fluxes that maritime low pressure systems draw upon as a source of energy. Second, the western North Pacific Ocean area has nearly an equal number of explosive and non-explosive storms, whereas the northwest Atlantic Ocean area has relatively few non-explosive events during this period. Since this research effort does not include other years, it is not known if this is an inherent feature of the region or a seasonal anomaly. Sanders and Gyakum (1980) found that the frequency of explosive cyclones occurring in the western North Pacific Ocean is slightly greater than in the western North Atlantic Ocean (see Figure 2.1). Finally, the average deepening rate for the Atlantic is greater than the Pacific average, as was evident in Sanders and Gyakum (1980).

The final list of cyclones in Table 1 is the subject of storm-environment mass and circulation budget diagnostics described in the next chapter. Comparisons and results of these derived quantities using all storms will be discussed in Chapter VI.

Table 1. Final list of cyclones and 24 h sea-level pressure changes (mb) not corrected for latitude. P and A denote explosive cyclones for the North Pacific Ocean and North Atlantic Ocean respectively. NP and NA denote non-explosive cyclones for the North Pacific Ocean and North Atlantic Ocean respectively.

PACIFIC

Explosive Cases

Lows	NMC	ECMWF	Date
P1	33	35	18 Jan 1979
P2	18	22	26 Jan 1979
P3	24	23	05 Feb 1979
P4 ^t	20	20	09 Feb 1979
P5	23	21	17 Feb 1979
P6	24	19	15 Feb 1979
P7	22	20	24 Jan 1979

Non-explosive

NP1	7	3	21 Jan 1979
NP2	13	15	31 Jan 1979
NP3	0	2	04 Feb 1979
NP4	5	2	04 Feb 1979
NP5	5	4	08 Feb 1979
NP6	16	11	13 Feb 1979
NP7	12	12	14 Feb 1979
NP8	18	11	21 Feb 1979
NP9	12	7	19 Feb 1979
NP10	21	16	13 Feb 1979
NP11	22	7	28 Jan 1979

ATLANTIC

Explosive Cases

A1	25	30	18 Jan 1979
A2	30	24	28 Jan 1979
A3	30	35	01 Feb 1979
A4	23	21	09 Feb 1979
A5	26	23	13 Feb 1979
A6	22	27	19 Feb 1979
A7	14	20	15 Feb 1979

Non-explosive

NA1	12	13	07 Feb 1979
NA2	5	11	22 Feb 1979
NA3	22	7	23 Jan 1979

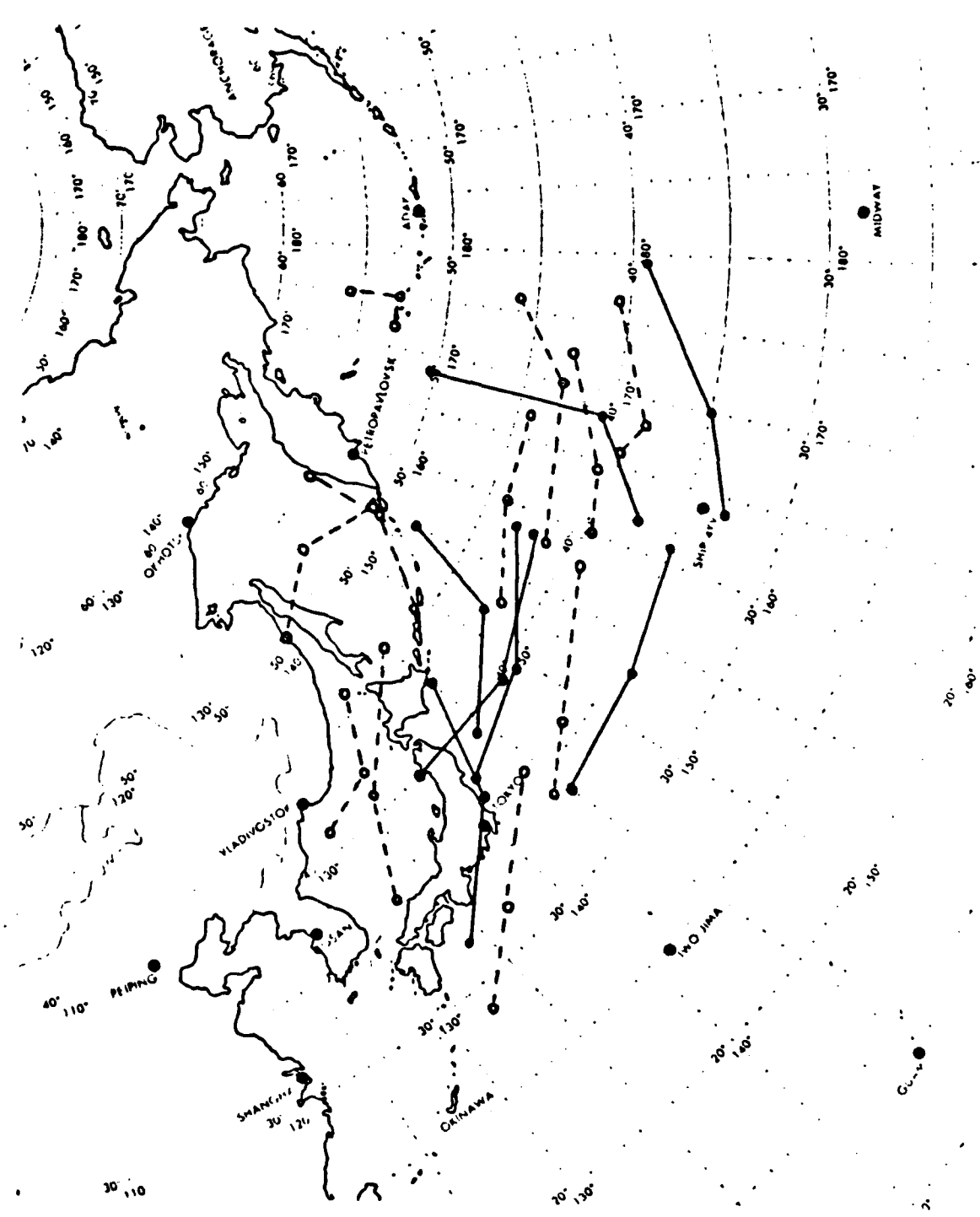


Fig. 4.1 Storm tracks and positions of the explosive and non-explosive cyclones in the North Pacific Ocean. Solid/dashed lines indicate tracks of explosive/non-explosive cyclones. Dots indicate initial, 12 h and 24 h positions.

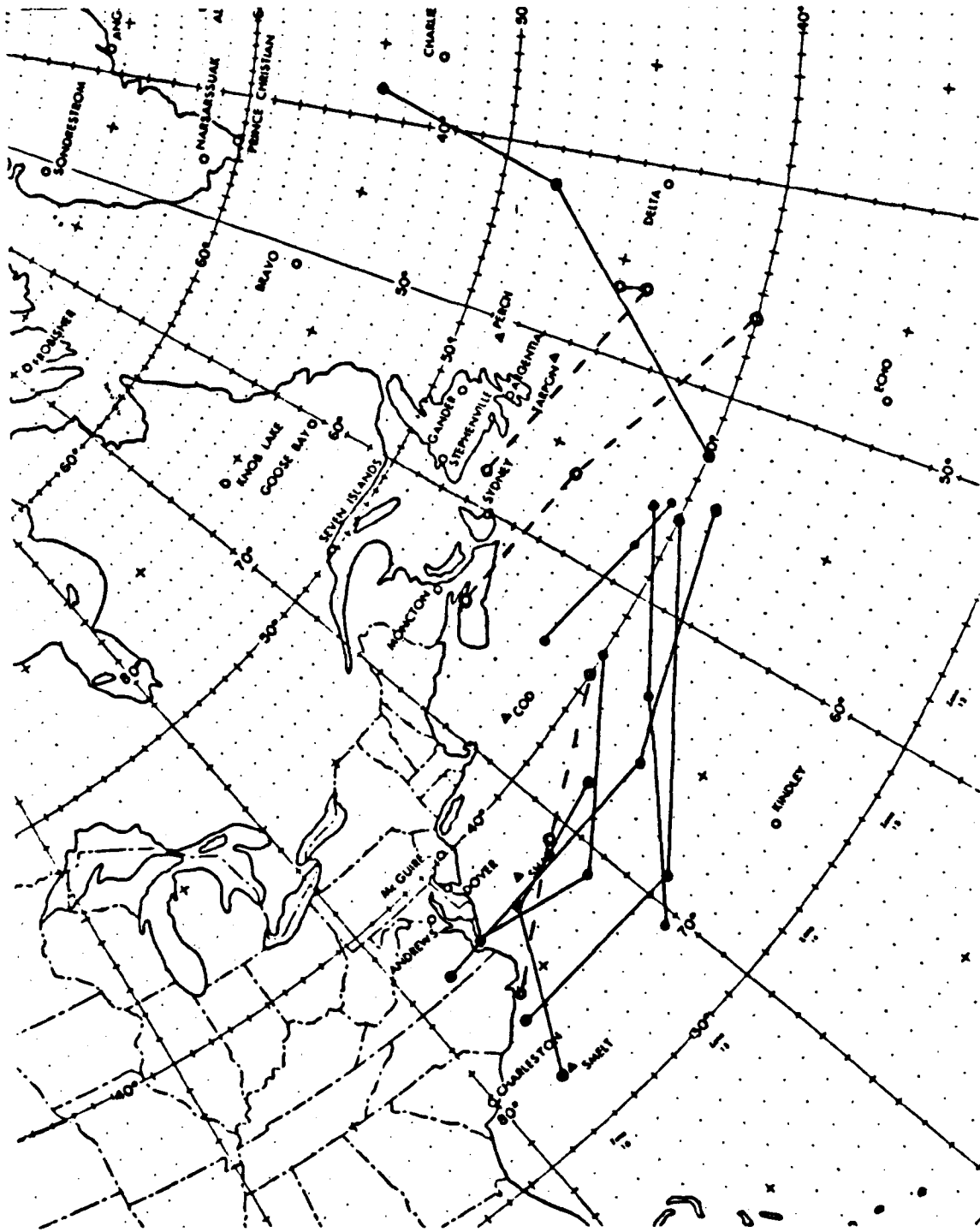


Fig. 4.2 Storm tracks and positions of the explosive and non-explosive cyclones in the North Atlantic Ocean. Solid/dashed lines indicate tracks of explosive/non-explosive cyclones. Dots indicate initial, 12 h and 24 h positions.

V. STORM-ENVIRONMENT DIAGNOSTIC CALCULATIONS

Fundamental in the investigation of extratropical cyclones is the necessity to resolve the processes responsible for their development. Calculations of storm-environment diagnostics (Wash, 1978; Johnson and Downey, 1975) are utilized in this thesis to study the two groups of cyclones. Inherent in this technique is the ability to calculate diagnostic statistics for the immediate cyclone area to describe the environment of the developing storm.

Past studies that used the quasi-Lagrangian technique (Cook, 1983; Calland, 1983; and others) resulted in complete budgets of storm properties, such as mass and vorticity, with the associated forcing terms. The intent was to investigate physical processes which are responsible for the changes in these properties throughout the entire life cycle of the cyclone. This study examines storm properties during the first 24 h of the life cycle of two different groups of cyclones. The motivation is to isolate the leading terms in the budgets during the early evolution. Processes which possibly are responsible for the deepening of cyclones are examined by studying the differences between explosive and non-explosive cyclones.

Calculation of storm-environment properties requires a separate coordinate system from the analysis grid. A spherical coordinate system is established which describes the earth. The storm-environment volume is centered over the minimum sea-level pressure of the cyclone. A reference radius is constructed through the center of the cyclone to the center of the earth. The radius of the storm-environment volume is perpendicular to the reference radius in increments of 1° latitude. Since the depth of the atmosphere is small compared to the earth radius, that portion of

the coordinate and grid system is treated as a cylinder. Further, the storm-environment volume is divided vertically into ten mandatory pressure levels and in the horizontal at radii of 1° latitude.

The terms which are used to describe the storm-environment are listed in Table 2. These properties are calculated using analyses every 12 h for three different periods during the life of the storm. Computational procedures are described for each property below.

Table 2. Storm-environment properties.

Absolute Vorticity
Vorticity Advection
Eddy Mode
Upper-Level Divergence
Mean Mode
Kinematic Vertical Velocity
Layer Average Potential Temperature
Static Stability

Paegle (1983) and others suggest not using the ECMWF Level III-b initialized temperature fields. To obtain analysis temperatures, layer temperatures are calculated from the thickness between two mandatory levels using the hypsometric equation. These layer temperatures are averaged for the horizontal cross section of the cylinder which encompasses the storm environment and are converted to potential temperatures. The static stability is defined as the change in the area-averaged layer potential temperature between two layers.

The absolute vorticity is computed for each mandatory pressure level. A layer-average absolute vorticity is

computed as the average between two levels after horizontally averaging over the cross-sectional area. The layer-averaged absolute vorticity advection is computed as the vector dot product of the wind and the gradient of the absolute vorticity at the two levels and then vertically averaged.

The horizontal transport of the absolute vorticity can be partitioned into a mean mode and an eddy mode (see Table 3). The eddy mode of the lateral transport of the absolute vorticity is similar to the advection of the absolute vorticity (Calland, 1983). The layer-average mean mode is determined after computing the boundary flux (line integral) the mean absolute vorticity and the normal component of the mean wind at two adjacent levels. The eddy mode is determined by subtracting the mean mode from the total transport of absolute vorticity. The total transport is calculated as the boundary flux (line integral) of the product of the absolute vorticity and normal wind component.

The kinematic vertical velocity is computed by vertically integrating the continuity equation in pressure coordinates. The divergence is calculated by computing the flux of mass at each level assuming zero mass fluxes at the surface and at 100 mb as boundary conditions. The lateral mass flux is computed from the wind fields and is balanced by the vertical mass flux due to the continuity of mass. Since errors exist in the wind measurements, a residual occurs when the horizontal mass flux is compared with the vertical mass flux. To assume mass continuity, the residual must be removed from each level. A weighting scheme by O'Brien (1970) is employed to distribute these corrections. A higher weighting is imposed in the upper troposphere due to larger inaccuracies in wind measurements. This results in a corrected horizontal mass flux.

The following chapter presents the results of the calculated storm-environment properties. The results emphasize the differences in the storm-environment quantities between the two cyclone groups.

Table 3. Partitioned lateral transport of absolute vorticity (after Calland, 1983).

The partitioned form of the vorticity budget equation is

$$\frac{\delta(C_a)}{\partial t} = + \text{LT}(\zeta_a) + \text{DVT}(\zeta_a) + S(\zeta_a)$$

┌──────────┴──────────┐
 mean mode eddy mode
 └──────────┬──────────┘
 horizontal divergence horizontal advection

 ┌──────────┴──────────┐
 vertical divergence vertical advection
 └──────────┬──────────┘
 divergence term tilting term

 ┌──────────┴──────────┐
 frictional dissipation

The above partitions make use of Stokes' theorem

$$\oint \zeta_a \underline{U} \cdot \underline{m} \, d\ell = \iint_A \nabla \cdot \zeta_a \underline{U} \, dA,$$

and the division of total flux ($\underline{U} \zeta_a$) into divergent and advective components,

$$\nabla \cdot \zeta_a \underline{U} = \zeta_a (\nabla \cdot \underline{U}) + \underline{U} \cdot \nabla \zeta_a.$$

VI. RESULTS

A. INTRODUCTION

Statistical studies of explosive cyclogenesis have been accomplished by Sanders and Gyakum (1980), Roebber (1984) and more recently by Rogers and Bosart (1985). Complete case studies of famous explosive cyclones, e.g. the Presidents' Day and Queen Elizabeth II storms have also been completed as summarized earlier. This study enlarges upon these case study results by diagnostically examining a group of 14 explosive cyclones and contrasting them to a set of 14 non-explosive systems. Data gathered during FGGE and analyzed by the ECMWF are used in the budget calculations. Storm properties are determined for radii of 4° and 6° latitude.

Comparisons of the averaged explosive and non-explosive storms are presented at the initial time of development ($t = 0$ h), mid-way through the 24 h deepening process ($t = 12$ h) and at the end of the deepening process ($t = 24$ h). Comparisons of the total 24 h average explosive and non-explosive storm characteristics are also included.

The thermal structure of both averaged storms is described by the static stability and the area-averaged layer potential temperature. The static stability is determined for layers 925 - 400 mb and 925 - 600 mb. The area-average layer potential temperature is presented at three different layers: 1000 - 850 mb, 1000 - 700 mb and 500 - 400 mb. Diagnostic terms to describe the upper-level forcing include vorticity advection, eddy and mean mode of vorticity transport, upper-level divergence and vertical motion. Mean and eddy modes of vorticity advection and upper-level divergence are computed for a layer from 500 mb to 200 mb. Kinematic vertical motion (ω) is given for

700 mb and the 450 mb level average. Low-level circulation is described by the absolute vorticity in the layers 1000 - 850 mb and 1000 - 700 mb.

Depicted in all tables are the mean quantities of the budget properties described above. Those quantities in parentheses below each mean value are the associated standard deviations. A student t-test is used with a 95% confidence interval to determine the statistical significance between the two cyclone groups for all storm properties. Those storm properties which meet the prescribed limits of the t-test are identified with a superscript 1 in all tables.

B. 24 H AVERAGE STORM COMPARISON

By investigating the initial 24 h of the cyclones development, key features that determine whether or not the surface low develops explosively will emerge. The three major areas of interest consist of the low-level circulation, upper-level forcing and the thermal structure of the storm groups.

Sea-level pressure statistics for both cyclone types are listed in Table 4 . The initial mean sea-level pressure for the explosive group is slightly higher than the non-explosive group, but this difference is not statistically significant. However, the average 24 h pressure change for the explosive group is nearly 23 mb and is only 9 mb for the non-explosive group. At the initial time, the low-level absolute vorticity values (Table 5) are in agreement with the initial sea-level pressures. That is, the absolute vorticity for the non-explosive storm group is larger than the explosive group. Significant differences are noted in the time tendencies of the average low-level absolute vorticity (Table 5) between the storm groups. The absolute vorticity for the explosive storm group increased by $71 \times 10^{-6} \text{ sec}^{-1}$ while the non-explosive group only increased by

$19 \times 10^{-6} \text{ sec}^{-1}$ for the 1000 - 850 mb layer (Table 5) at radius 4° latitude.

The 24 h average upper-level forcing diagnostics (Table 6) indicate significantly stronger upper-level support for the explosively developing cases. Consistent with all developing storms, vorticity advection is positive for both groups. However, the positive vorticity advection associated with the average explosive cyclone is nearly twice the amount of the average non-explosive cyclone at both radii. This supports the relationship found between mid-level short waves lagging approximately 400 n mi behind the explosive surface lows (Sanders and Gyakum, 1980). The eddy mode, which is analogous to advection of vorticity, as described in Chapter V, is consistent with the vorticity advection results. Upper-level divergence is nearly twice as large for the average explosive storm as for the non-explosive storm. With greater divergence aloft larger surface pressure falls are found for the average explosive storm. The upper-level mean mode, which is similar to the divergence term of the vorticity equation, displays the same trends as the upper-level divergence.

Compensation for the greater mass divergence at the upper levels is reflected by larger upward vertical motion experienced by the average explosive low (Table 7). The explosive group average vertical motion is approximately 60% larger than for the non-explosive group for either layer. Furthermore, the variability of the data for the explosive storm is lower than for the non-explosive storm. The 24 h average 700 mb vertical velocity is larger for both storm groups than at the 450 mb level which implies that the level of non-divergence possibly could be the same for both storm groups.

The static stabilities (Table 8) surprisingly do not indicate less stability for the explosive cyclone group.

Both storm types also display nearly the same variability about the mean. The important difference that exists at both radii and for each layer is that the area-averaged layer potential temperature for the explosive case is approximately 4° K higher than for the non-explosive case. The higher potential temperature associated with the average explosive system suggests that the surface perturbation develops on the warm side of the baroclinic zone. Furthermore, higher temperatures associated with the explosive lows indicate a potentially greater source of moisture for the explosive system. The average latitudes during the development stage are 39° N and 43° N for the average explosive and non-explosive cases respectively (see Figures 4.1 and 4.2), which is reflected in the difference between their mean potential temperatures. The area-average potential temperature variability of each storm group is nearly the same at both radii.

C. TIME TENDENCY OF LOW-LEVEL CIRCULATION

Absolute vorticity was computed for two layers and at radius 4 and radius 6 (Table 5). The trends for both average cases show an increase in absolute vorticity, especially for 1000 - 850 mb. Although initially ($t = 0$ h) the non-explosive cyclone absolute vorticity is greater than for the explosive case, the explosive low displays a greater growth and the vorticities by 24 h are greater than for the non-explosive low. This larger increase of absolute vorticity displayed by the explosive low is indicative of the rapid growth process of the low-level perturbation and is in agreement with the sea-level pressure statistics. The weaker initial vorticity values (as well as sea-level pressure values) for the explosive systems suggests these systems are not initially more intense in the low troposphere.

D. TIME TENDENCY OF UPPER-LEVEL FORCING

The vorticity advection calculations do not show the explosive cyclones have significantly greater positive vorticity advection at $t = 0$ h. Notice the high standard deviation at 0 h compared to 12 h and 24 h. This variability probably indicates that the surface low at 0 h is sometimes actually well into a positive vorticity region and other times is actually prior to the rapid deepening stage. Given the 12 h time resolution, a more precise evolution cannot be defined. Additionally, this could be the result of the layer averaging process of the diagnostic technique. For example, if strong positive vorticity advection existed upstream of the surface cyclone but it is averaged with negative vorticity advection downstream, the net effect may mask the strength of the upstream positive vorticity. Thus, the upstream positive vorticity advection may not be totally accounted for in the storm-centered averages. Another explanation may be that extremely rapid self-development occurs during the first 12 h period and produces the rapid positive vorticity advection increase. Further diagnostic calculations should answer this question.

Vorticity advection is positive and strongest during the first 12 h for both cases and at either radii. Comparing magnitudes at each time period, the explosive storm consistently imports greater vorticity aloft than does the non-explosive case. This results in greater upper-level divergence, which thereby increases sea-level pressure falls. By contrast, the vorticity advection (and eddy mode of vorticity transport) for the non-explosive system remains steady over the 24 h period. The 24 h average value is actually less than the $t = 0$ h value. There is a significant difference at the 12 h mark between explosive and non-explosive systems. It is unclear why the vorticity advection average in the explosive cases drops at 24 h. The

variability is higher at 24 h, which suggests that periods of upper-level forcing in some cases may not extend for 24 h. The locations of the lows, which are farther from the coastal data at this time, may be a factor. Similar trends are observed at radius 6 (Table 10), although the magnitudes of vorticity advection are proportionately smaller. The results of the eddy mode calculations again follow the vorticity advection results.

Similar trends are exhibited in the upper-level divergence (Table 9 and 10). Consistent with the vorticity advection trends, the upper-level divergence is greater for the average explosive group at all time increments. Notice the upper-level divergence of the explosive systems is only marginally larger than the non-explosive systems at $t = 0$ h and the upper-level divergence also has smaller $t = 24$ h values. Comparing divergence magnitudes at each time increment (0 h, 12 h, 24 h), the average explosive cyclone steadily increases relative to the average non-explosive cyclone. For time 0 h, 12 h, and 24 h the average explosive low was 35%, 47% and 50%, respectively, greater in magnitude than the non-explosive low. The upper-level divergence for the average non-explosive case actually decreased while the divergence in the average explosive case increased by nearly 20 percent. At radius 6, the same trends are experienced.

The mean mode, which reflects the outward vorticity transport due to mean divergence aloft, is consistent with the trends exhibited by the upper-level divergence (Tables 9 and 10). Since the upper-level divergence is significantly greater for the average explosive low than for the non-explosive low, sea-level pressure falls for the explosive low are greater than the non-explosive low. Furthermore, this dynamical effect is reflected in the increasing trend of the low-level absolute vorticity for both cyclone groups (Table 5).

The kinematic vertical velocities (Tables 11 and 12) display slightly different trends than those exhibited by all of the other upper-level forcing functions. The upward vertical motion at 450 mb displays an increase at all time increments for the average explosive low. The explosive storm shows more variability than the non-explosive storm during the initial period. At 12 h, the variability of both storm groups are nearly equal and by the end of the development period the explosive storm shows less variability than the non-explosive storm. The explosive system has significantly larger vertical motion at $t = 12$ h and 24 h for both radius 4 and 6 latitude.

Vertical motion at 700 mb remains nearly constant for the non-explosive group. The initial vertical velocities of the explosive cyclones is higher (by 15%), although this difference is not statistically significant. By 12 h, the vertical motion associated with the explosive group is 75% larger than for the non-explosive set. At radius 6, the same trends are exhibited by the explosive cyclone however the non-explosive cyclone displays a net decrease. Vertical motions for both storm groups are greater at 700 mb than at the upper levels. This suggests that both types of cyclones are shallow at this stage of development.

The obvious feature that stands out for all upper-level forcing statistics is the overwhelming relative strength of the average explosive cyclone properties (see Tables 9 and 10). This is true for each time increment and either radius. In nearly all aspects of upper-level forcing, both cyclone groups exhibit a rapid increase in storm properties during the first 12 h of development. During the second 12 h period, both storms nearly always show a slight decrease in storm properties. This increase-decrease trend for the first and second 12 h periods could be the result of less data in the analyses at the 24 h analysis (cyclone further

from the coast). In many cases, the average non-explosive low will exhibit a lower value at the end of the 24 h period than at the beginning. This trend could possibly be due to the maturation of the storm. A trend such as this could imply that there is a period of perhaps 12 h of strong upper-level forcing. However, the limited time resolution of the analyses cannot resolve this point.

E. TIME TENDENCY OF THE THERMAL STRUCTURE

The trends in the static stability indicate no substantial stabilizing or destabilizing effect within the 24 h time period (Table 13) for either storm group. Static stability differences between the storms are so small that no inferences can be made. This result is also evident for either layer and either radius (Table 14). The variability of the static stability data is nearly equal for both storms.

More significantly, the layer potential temperature associated with the explosive storm is higher than the non-explosive storm at each layer and at each time period. Additionally, the average explosive low displays a slight cooling trend (of several degrees) during the second 12 h period at all layers and radii. This suggests the migration of the explosive low pressure system from the warm side to the cold side of the baroclinic zone as the storm rapidly deepens and begins to wrap around itself. This cooling trend is not evident for the non-explosive case. The variability in the layer potential temperature for the explosive storms tends to be less than for the non-explosive cases.

F. SUMMARY

The major differences between the explosive cyclones and non-explosive cyclones were found in the upper-level characteristics of the storms. Static stability analyses revealed no substantial differences and no stability trends between

the storms. The area-average potential temperatures of the explosive storm displayed higher values relative to the non-explosive storm. The overwhelming upper-level support associated with the average explosive low is indicative of the rapid deepening inherent with these systems. Kinematic vertical velocities demonstrate the three-dimensional consistency of the data set as well as the dynamics associated with both cases. Initially there are no significant differences in low-level absolute vorticity between the explosive storm and the non-explosive storm. However, the explosive group displays a steady growth and by the end of the time period, the vorticities have substantially increased relative to those for the non-explosive group. The consistent growth of the low-level vorticity exhibited by the average explosive low supports the results of all of the above physical characteristics.

Table 4. 24 h average low-level circulation features for both storm groups at radii 4° and 6° latitude.

	<u>Explosive</u>	<u>Non-Explosive</u>
Initial Central Sea-level Pressure (mb)	1006.1 (8.1)	1004.6 (8.5)
24 h Surface Pressure Change (mb)	22.67 ¹ (8.2)	8.78 ¹ (4.8)

Table 5. 24 h time evolution of low-level absolute vorticity for both storm groups at radii 4° and 6° latitude.

	Radius 4		Radius 6	
	<u>Explosive</u>	<u>Non-Explosive</u>	<u>Explosive</u>	<u>Non-Explosive</u>
Absolute Vorticity ($\times 10^{-6}$ sec $^{-1}$)				
1000 - 850 mb				
t = 0 h	104 ¹ (31)	128 ¹ (25)	101 ¹ (13)	115 ¹ (22)
t = 12 h	139 (18)	139 (23)	125 (28)	122 (19)
t = 24 h	175 ¹ (33)	147 ¹ (25)	136 ¹ (14)	130 ¹ (17)
1000 - 700 mb				
t = 0 h	221 (28)	250 (52)	203 (27)	230 (64)
t = 12 h	278 (36)	265 (48)	233 (38)	248 (42)
t = 24 h	319 (67)	293 (51)	278 (31)	254 (48)

Table 6. 24 h average upper-level forcing properties of both storm groups for the layer 500 - 400 mb at radii 4° and 6° latitude.

	Radius 4		Radius 6	
	<u>Explosive</u>	<u>Non-Explosive</u>	<u>Explosive</u>	<u>Non-Explosive</u>
500 - 200 mb				
Vorticity Advection ($\times 10^{-5}$ sec $^{-2}$)	738 ¹ (276)	417 ¹ (210)	483 ¹ (171)	277 ¹ (124)
Eddy Mode ($\times 10^{-5}$) sec $^{-2}$	756 ¹ (294)	444 ¹ (241)	508 ¹ (182)	297 ¹ (132)
Mean Mode ($\times 10^{-5}$ sec $^{-2}$)	-528 ¹ (157)	-299 ¹ (174)	-343 ¹ (147)	-217 ¹ (120)
Upper-Level Mass Divergence ($\times 10^{-5}$ g/sec)	-1894 ¹ (585)	-1036 ¹ (522)	-2827 ¹ (922)	-1721 ¹ (766)

Table 7. 24 h average kinematic vertical motion for both storm groups.

Omega ($\times 10^{-5}$ mb/sec)	Radius 4		Radius 6	
	<u>Explosive</u>	<u>Non-Explosive</u>	<u>Explosive</u>	<u>Non-Explosive</u>
450 mb	-302 ¹ (83)	-187 ¹ (100)	-219 ¹ (70)	-146 ¹ (82)
700 mb	-365 ¹ (125)	-224 ¹ (93)	-253 ¹ (92)	-184 ¹ (91)

Table 8. 24 h average thermal structure for both storm groups.

	Radius 4		Radius 6	
	<u>Explosive</u>	<u>Non-Explosive</u>	<u>Explosive</u>	<u>Non-Explosive</u>
Static Stability (d0/dp) ($\frac{K}{100 \text{ mb}}$)				
925 - 400 mb	-4.83 (0.66)	-4.91 (0.78)	-5.03 (0.60)	-5.10 (0.75)
925 - 600 mb	-4.25 (0.95)	-4.58 (1.51)	-4.39 (0.97)	-4.80 (1.52)
³ Potential Temperature ($^{\circ}$ K) (Layer Averaged)				
1000 - 850 mb	284.0 (3.4)	279.9 (6.6)	282.9 (3.3)	278.9 (6.7)
1000 - 700 mb	287.2 (3.4)	283.3 (6.7)	286.3 (3.3)	282.6 (6.8)
500 - 400 mb	306.8 (4.4)	303.2 (8.0)	306.7 (4.1)	303.2 (7.7)

Table 9. 24 h time evolution of upper-level properties at radius 4° . Values are averaged for the layer 500 - 200 mb for both storm groups.

	<u>Explosive</u>	<u>Non-Explosive</u>
Vorticity Advection ($\times 10^{-11}$ sec $^{-2}$)		
t = 0 h	555 (663)	423 (360)
t = 12 h	859 ¹ (412)	459 ¹ (429)
t = 24 h	688 (601)	326 (400)
Eddy Mode ($\times 10^{-11}$ sec $^{-2}$)		
t = 0 h	545 (668)	470 (289)
t = 12 h	857 (471)	482 (489)
t = 24 h	763 (631)	342 (406)
Mean Mode ($\times 10^{-11}$ sec $^{-2}$)		
t = 0 h	-367 (160)	-206 (250)
t = 12 h	-592 ¹ (250)	-311 ¹ (244)
t = 24 h	-563 ¹ (206)	-315 ¹ (269)
Upper-Level Mass Divergence ($\times 10^{-11}$ g/sec)		
t = 0 h	-1564 (939)	-1023 (577)
t = 12 h	-2022 ¹ (788)	-1069 ¹ (744)
t = 24 h	-1970 ¹ (734)	-984 ¹ (676)

Table 10. 24 h time evolution of upper-level properties at radius 6. Values are averaged for the layer 500 - 200 mb for both storm groups.

	<u>Explosive</u>	<u>Non-Explosive</u>
Vorticity Advection ($\times 10^{-11}$ sec $^{-2}$)		
t = 0 h	363 (462)	269 (203)
t = 12 h	544 ¹ (262)	315 ¹ (222)
t = 24 h	482 ¹ (300)	210 ¹ (270)
Eddy Mode ($\times 10^{-11}$ sec $^{-2}$)		
t = 0 h	372 (472)	274 (214)
t = 12 h	558 ¹ (285)	343 ¹ (227)
t = 24 h	543 ¹ (316)	229 ¹ (274)
Mean Mode ($\times 10^{-11}$ sec $^{-2}$)		
t = 0 h	-220 (86)	-186 (145)
t = 12 h	-380 ¹ (192)	-234 ¹ (158)
t = 24 h	-392 ¹ (186)	-213 ¹ (148)
Upper-Level Mass Divergence ($\times 10^{-11}$ g/sec)		
t = 0 h	-2210 (1056)	-1730 (819)
t = 12 h	-3052 ¹ (1168)	-1762 ¹ (1041)
t = 24 h	-2993 ¹ (1061)	-1630 ¹ (892)

Table 11. 24 h time evolution of kinematic vertical motion at radius 4° for both storm groups.

Omega ($\times 10^{-3}$ mb/sec)	<u>Explosive</u>	<u>Non-Explosive</u>
450 mb		
t = 0 h	-236 (125)	-173 (94)
t = 12 h	-321 ¹ (134)	-194 ¹ (134)
t = 24 h	-331 ¹ (109)	-188 ¹ (133)
700 mb		
t = 0 h	-271 (149)	-226 (109)
t = 12 h	-392 ¹ (180)	-224 ¹ (137)
t = 24 h	-374 ¹ (118)	-221 ¹ (110)

Table 12. 24 h time evolution of kinematic vertical motion at radius 6° for both storm groups.

Omega (*10 ⁻³ mb/sec)	<u>Explosive</u>	<u>Non-Explosive</u>
450 mb		
t = 0 h	-163 (67)	-137 (86)
t = 12 h	-234 ¹ (91)	-151 ¹ (99)
t = 24 h	-247 ¹ (83)	-146 ¹ (85)
700 mb		
t = 0 h	-198 (67)	-183 (90)
t = 12 h	-293 ¹ (130)	-191 ¹ (120)
t = 24 h	-264 ¹ (83)	-171 ¹ (84)

Table 13. 24 h time evolution of the thermal structure for both storm groups at radius 4° .

	<u>Explosive</u>	<u>Non-Explosive</u>
$d\theta/dp$ ($^\circ$ K/100 mb)		
925 - 400 mb		
t = 0 h	-4.87 (0.79)	-4.98 (1.23)
t = 12 h	-4.75 (0.78)	-4.93 (0.79)
t = 24 h	-4.96 (0.73)	-4.80 (0.75)
925 - 600 mb		
t = 0 h	-4.06 (1.54)	-5.09 (1.47)
t = 12 h	-4.33 (0.96)	-4.43 (2.14)
t = 24 h	-4.27 (2.32)	-4.37 (1.40)
Layer Temperature ($^\circ$ K)		
1000 - 850 mb		
t = 0 h	284.0 (5.0)	280.0 (7.3)
t = 12 h	284.7 (3.5)	279.9 (7.3)
t = 24 h	282.7 (4.6)	279.8 (6.1)
1000 - 700 mb		
t = 0 h	287.0 (5.1)	283.7 (7.4)
t = 12 h	287.9 (3.5)	283.2 (7.4)
t = 24 h	285.9 (4.2)	283.0 (6.2)

Table 13. (continued).

Layer Temperature ($^{\circ}$ K)	<u>Explosive</u>	<u>Non-Explosive</u>
500 - 400 mb		
$t = 0$ h	307.3 (7.1)	303.6 (9.8)
$t = 12$ h	307.1 (4.7)	303.3 (7.9)
$t = 24$ h	306.3 (4.5)	302.6 (7.4)

Table 14. 24 h time evolution of the thermal structure for both storm groups at radius 6°.

	<u>Explosive</u>	<u>Non-Explosive</u>
$d\theta/dp$ ($^{\circ}$ K/100 mb)		
925 - 400 mb		
t = 0 h	-5.09 (0.75)	-5.18 (1.04)
t = 12 h	-4.95 (0.67)	-5.09 (0.82)
t = 24 h	-5.13 (0.63)	-5.03 (0.71)
925 - 600 mb		
t = 0 h	-4.28 (1.46)	-5.22 (1.39)
t = 12 h	-4.41 (1.04)	-4.60 (2.07)
t = 24 h	-4.45 (1.82)	-4.79 (1.23)
Layer Temperature ($^{\circ}$ K)		
1000 - 850 mb		
t = 0 h	283.1 (5.0)	279.2 (7.2)
t = 12 h	283.7 (3.3)	279.0 (7.4)
t = 24 h	281.4 (4.5)	278.5 (6.3)
1000 - 700 mb		
t = 0 h	286.7 (4.6)	283.2 (7.5)
t = 12 h	286.8 (3.3)	279.0 (7.5)
t = 24 h	284.7 (4.2)	282.1 (6.3)

Table 14. (continued).

Layer Temperature ($^{\circ}$ K)	<u>Explosive</u>	<u>Non-Explosive</u>
500 - 400 mb		
$t = 0$ h	307.3 (7.1)	303.6 (9.8)
$t = 12$ h	307.1 (4.7)	303.3 (7.9)
$t = 24$ h	306.3 (4.5)	302.6 (7.4)

VII. CONCLUSIONS AND RECOMMENDATIONS

To gain further insight into maritime rapid cyclogenesis, storm-environment properties of explosive and non-explosive cyclones are compared. Both types of storms are selected during the period 17 January 1979 to 23 February 1979. Storm-environment properties are computed from ECMWF Level III-b analyses of FGGE data. Differences between cyclone groups and time trends through the initial 24 h deepening period are examined. The following conclusions are made from this collection of explosive and non-explosive developing cyclones.

The initial low-level perturbations for both storm types are of nearly equal intensity, as reflected by the sea-level pressure and low-level absolute vorticity statistics. In fact, the non-explosive set is slightly stronger (high absolute vorticity and lower sea-level pressure). Upper-level properties display the most significant differences and trends between the storm types. Positive vorticity advection, eddy mode vorticity export and upper-level divergence associated with the explosive group are dramatically greater. Kinematic vertical velocities also follow the upper-level terms and demonstrate the consistency of both data sets. Maximum kinematic vertical velocities are greater at 700 mb than at 450 mb.

Neither storm type displays a destabilizing trend. Static stabilities are low and remain unchanged through the first 12 h period for both storm types. A slight stabilizing trend is evident during the second 12 h period for both storms.

In future research, the sample size of both types of cyclones should be increased to provide additional statistical significance in each storm property. To reduce the

masking effect due to the horizontal averaging of the total storm-environment the quadrants about the storm center should be analyzed to determine the horizontal distribution of these characteristics. Other important factors such as low-level moisture and thermal advection also should be computed. Analyses of jet streak positions and their dynamic interactions associated with explosive deepening processes should be investigated further.

The physical processes that cause rapid cyclogenesis over the open ocean must be fully understood by the forecaster. Improved observational networks and numerical weather prediction techniques are needed. Until then, maritime explosive cyclogenesis remains a challenge to the forecaster and a great threat to the mariner.

LIST OF REFERENCES

- Anthes, R. A., Y. H. Kuo, and J. R. Gyakum, 1983: Numerical simulation of a case of explosive maritime cyclogenesis. Mon. Wea. Rev., 100, 1174-1188.
- Bengtsson, L., M. Kanamitsu, P. Kallberg, and S. Uppala, 1982: FGGE 4-dimensional data assimilation at ECMWF. Bull. Amer. Meteor. Soc., 63, 29-43
- Bjorheim, K., P. Julian, M. Kanamitsu, P. Kallberg, P. Price, S. Tracton, and S. Uppala, 1981: FGGE III-B Daily Global Analyses - 4 Parts. European Centre for Medium-range Weather Forecasts, Reading, U. K.
- Bosart, L. F., 1981: The Presidents' Day snowstorm of 18-19 February 1979: A subsynoptic scale event. Mon. Wea. Rev., 109, 1542-1566
- Bosart, L. F., and S. C. Lin, 1984: A diagnostic analysis of the Presidents' Day storm of February 1979. Mon. Wea. Rev., 112, 2148-2177
- Calland, W. E., 1983: Quasi-Lagrangian diagnostics applied to an extratropical explosive cyclogenesis in the North Pacific. M.S. Thesis, Naval Postgraduate School, 154 pp.
- Chang, C. B., D. J. Perkey and C. W. Kreitzberg, 1984: Latent heat induced energy transformations during cyclogenesis. Mon. Wea. Rev., 112, 357-366.
- Chen, T.-S., C.-B. Chang, and D. J. Perkey, 1985: Synoptic study of a medium-scale oceanic cyclone during AMTEX 75. Mon. Wea. Rev., 113, 349-361.
- Cook, W. A., 1983: A quasi-Lagrangian diagnostic investigation of rapid cyclogenesis in a polar air stream. M.S. Thesis, Naval Postgraduate School, 147 pp.
- Gyakum, J. R., 1983a: On the evolution of the QE-II Storm. I: Synoptic aspects. Mon. Wea. Rev., 111, 1137-1155.
- Gyakum, J. R., 1983b: On the evolution of the QE-II Storm. II: Dynamic and thermodynamic structure. Mon. Wea. Rev., 111, 1156-1173.
- Halem, M., E. Kalnay, W. E. Baker, and R. Atlas, 1982: An assessment of the FGGE satellite observing system during SOP-I. Bull. Amer. Meteor. Soc., 63, 407-427.

- Johnson, D. R., and W. K. Downey, 1975: Azimuthally averaged transport and budget equations for storms: Quasi-Lagrangian Diagnostics. Mon. Wea. Rev., 103, 967-979.
- O'Brien, J. J., 1970: Alternative solutions to the classical vertical velocity problem. J. Appl. Meteor., 2, 197-203.
- Ooyama, K., 1969: Numerical Simulation of the life cycle of tropical cyclone. J. Atmos. Sci., 26, 3-40.
- Paegle, J., 1983: Some characteristics of ECMWF Level III-b data sets. Global Weather Experiment Newsletter, 1, May 1983.
- Pagnotti, V., and L. F. Bosart, 1984: Comparative diagnostic case study of east coast secondary cyclogenesis under weak versus strong synoptic-scale forcing. Mon. Wea. Rev., 112, 5-30.
- Petterssen, S., 1956: Weather Analysis and Forecasting, Vol. 1, Motion and Motion Systems. McGraw-Hill, 428 pp.
- Roebber, P. J., 1984: Statistical analysis and updated climatology of explosive cyclogenesis. Mon. Wea. Rev., 112, 1577-1589.
- Rogers, E., and L. F. Bosart, 1985: An investigation of explosive deepening oceanic cyclones. To appear in Mon. Wea. Rev.
- Sanders, F., and J. R. Gyakum, 1980: Synoptic-dynamic climatology of the "Bomb". Mon. Wea. Rev., 108, 1589-1606.
- Uccellini, L. W., 1984: Comments on "Comparative diagnostic case study of east coast secondary cyclogenesis under weak versus strong synoptic-scale forcing." Mon. Wea. Rev., 112, 2540-2543.
- Uccellini, L. W., P. J. Kocin, R. A. Peterson, C. H. Wash, and K. F. Brill, 1984: The Presidents' Day cyclone of 18-19 February 1979: Synoptic overview and analysis of the subtropical jet streak influencing the pre-cyclogenetic period. Mon. Wea. Rev., 112, 31-55.
- Uccellini, L. W., D. Keyser, K. F. Brill, and C. H. Wash, 1985: The Presidents' Day cyclone of 18-19 February 1979: Amplification and associated tropopause folding on rapid cyclogenesis. Mon. Wea. Rev., 113, 962-988.

Wash, C. H., 1978: Diagnostics of observed and numerically simulated extratropical cyclones. Ph.D. Thesis, Department of Meteorology, University of Wisconsin, 215 pp.

INITIAL DISTRIBUTION LIST

		No.	Copies
1.	Defense Technical Information Center Cameron Station Alexandria, VA 22304-6145		2
2.	Library, Code 0142 Naval Postgraduate School Monterey, CA 93943		2
3.	Chairman (Code 63Rd) Department of Meteorology Naval Postgraduate School Monterey, CA 93943		1
4.	Chairman (Code 68Mr) Department of Oceanography Naval Postgraduate School Monterey, CA 93943		1
5.	Professor C. Wash (Code Wx) Department of Meteorology Naval Postgraduate School Monterey, CA 93943		7
6.	Professor R. Elsberry (Code Es) Department of Meteorology Naval Postgraduate School Monterey, CA 93943		1
7.	LCDR Darrell H. Smith 2313 Louise Lane Norman, OK 73071		2
8.	Director Naval Oceanography Division Naval Observatory 34th and Massachusetts Avenue NW Washington, DC 20390		1
9.	Commander Naval Oceanography Command NSTL Station Bay St. Louis, MS 39522		1
10.	Commanding Officer Naval Oceanographic Office NSTL Station Bay St. Louis, MS 39522		1
11.	Commanding Officer Fleet Numerical Oceanography Center Monterey, CA 93943		1
12.	Commanding Officer Naval Ocean Research and Development Activity NSTL Station Bay St. Louis, MS 39522		1
13.	Commanding Officer Naval Environmental Prediction Research Facility Monterey, CA 93943		1

- | | | |
|-----|---|---|
| 14. | Chairman, Oceanography Department
U.S. Naval Academy
Annapolis, MD 21402 | 1 |
| 15. | Chief of Naval Research
Naval Ocean Research and Development Activity
800 N. Quincy Street
Arlington, VA 22217 | 1 |
| 16. | Office of Naval Research (Code 420)
Naval Ocean Research and Development Activity
800 N. Quincy Street
Arlington, VA 22217 | 1 |
| 17. | Scientific Liason Office
Office of Naval Research
Scripps Institution of Oceanography
La Jolla, CA 92037 | 1 |
| 18. | Dr. James F. Kimpel
Dept. of Meteorology
University of Oklahoma
Norman, OK 73071 | 1 |
| 19. | Commander
Oceanographic Systems Pacific
Box 1390
Pearl Harbor, HI 96860 | 1 |
| 20. | Commanding Officer
Naval Eastern Oceanography Center
Naval Air Station
Norfolk, VA 23511 | 1 |
| 21. | Commanding Officer
Naval Western Oceanography Center
Box 113
Pearl Harbor, HI 96860 | 1 |
| 22. | Commanding Officer
Naval Oceanography Command Center, Rota
Box 31
FPO San Francisco, CA 09540 | 1 |
| 23. | Commanding Officer
Naval Oceanography Command Center, Guam
Box 12
FPO San Francisco, CA 96630 | 1 |

END

DTIC

6-86